XI International Conference on Computational Plasticity. Fundamentals and Applications
COMPLAS XI
E. Oñate, D.R.J. Owen, D. Peric and B. Suárez (Eds)

A DUAL MORTAR-BASED CONTACT FORMULATION APPLIED TO FINITE PLASTIC STRAINS – COMPLAS XI

T. Doca, F.M. Andrade Pires and J.M.A. César de Sá

Department of Mechanical Engineering (DEMec)
Faculty of Engineering
University of Porto, Porto, Portugal
e-mail: thiago.doca@fe.up.pt

Key words: Dual mortar method, active set strategy, finite plastic deformation.

Abstract. Significant progress has been made on computational contact mechanics over the past decade. Many of the drawbacks that were inherent to the standard node-to-segment element strategy, such as locking/over-constraint and non-physical jumps in the contact forces due to the discontinuity of the contact surface, have been systematically overcome. In particular, the formulation of the mortar finite element method [1], which has allowed the establishment of efficient segment-to-segment approaches [2, 3] when applied to the discretization of a contact surface, has promoted significant advance. However, the regularization schemes used with the mortar element (e.g. the Penalty method, the Lagrange multipliers method or combination of them) still cause unwanted side-effects such as: ill-conditioning, additional equations in the global system or a significant increase in the computational time for solution. In order to circumvent these shortcomings, Wohlmuth [4] has proposed the use of dual spaces for the Lagrange multipliers allowing the local elimination of the contact constraints. As a consequence, the Lagrangian multipliers can be conveniently condensed and no additional equations are needed for the solution of the global system of equations. H́ueber et al. [5], Hartmann et al. [6], Popp et al.[7] and Gitterle et al [8]. have later combined this methodology with an active set strategy and obtained improved results in terms of convergence rate. Despite the successful application of the dual mortar formulation to contact problems, the advances presented in the literature have, to the authors knowledge, only been employed for the simulation of elastic problems. However, contact between bodies has a strong influence in many applications (e.g., metal forming and cutting) where finite inelastic strains play a crucial role. Therefore, the main goal of the present work is both the application and assessment of the dual mortar method in problems where contact takes place coupled with finite plastic strains.

1 INTRODUCTION

The great majority of industrial processes involve plastic deformation of metallic bodies. There are several manufacturing procedures to modify the shape (i.e. Extrusion, U-Shaping, L-Shaping, Upsetting, etc) and they all share a common mechanism: the frictional contact. The correct prediction of frictional forces is intimately related to the precise computation of the normal contact forces. One of the most common methods to solve a non-conforming contact contact problem is the standard node-to-segment Lagrangian method. However the drawbacks inherent to the node-to-segment (NTS) approach, such as locking/over-constraint and non-physical jumps in the contact forces due to the discontinuity of the contact surface, use to compromise the method's results. Therefore, it is possible to replace the strong pointwise non-penetration function by a weaker integral condition through the use of dual spaces for the Lagrange multiplier [4]. This provides a very efficient discretization approach for non-conforming meshes, and therefore, a more accurate evaluation of the normal contact forces. The main goal in this work is to assess how the Dual Mortar method behaves when the deformation field along the contact surface evolves to the plastic zone. This paper is organized as follows: in Section 2, the contact problem is presented by stating the boundary conditions, the contact kinematics and the material model employed. In Section 3, the final equation system of the Dual Mortar method is presented. Numerical examples comparing the Dual Mortar method and the lagrangian method, are given in Section 4. Conclusion remarks are presented in Section 5.

2 PROBLEM DEFINITION

Considering two solid bodies in the reference configuration, we denote them by Ω^s and Ω_m, $\{\Omega_s \cup \Omega_m = \Omega : \Omega \subset \mathbb{R}^2\}$. The boundaries of subset Ω are divided in a contact zone Γ_c, a Neumann part Γ_N and a Dirichlet part Γ_D, $\{\Gamma_c \cup \Gamma_N \cup \Gamma_D = \Gamma : \Gamma \subset \mathbb{R}\}$. It is assumed that Γ_D has a non-zero measure. The boundary value problem, in terms of the displacement vector $\mathbf{u}$, is given as follows:

$$-\nabla \cdot (\sigma(\mathbf{u})) = f \ in \ \Omega, \tag{1}$$

$$\mathbf{u} = 0 \ on \ \Gamma_D \tag{2}$$

$$\sigma(\mathbf{u})\,\mathbf{n} = \mathbf{t}, \tag{3}$$

where f is the body forces over Ω and $\mathbf{t}$ are the prescribed tractions on the Neumann boundary. The outward unit normal vector $\mathbf{n}$ on Γ_c is defined with respect to the slave body Ω_s. The stress tensor σ is obtained using the classical von Mises nonlinear model. The yield function for the von Mises criterion can be defined as:

$$\Phi(\sigma) = \sqrt{J_2\left(\mathcal{S}\left(\sigma\right)\right)} - \tau_y, \tag{4}$$

with J_2 as the second principal invariant of the deviatoric stress tensor $\mathcal{S} = \sigma - p\mathbf{I}$, where p is hydrostatic pressure, and τ_y as the shear stress tensor. The gap function $g(\mathbf{X}, t)$ is

defined as the normal distance between a point $\mathbf{x}^{(1)}$ over the slave surface (Γ_s) and a point $\mathbf{x}^{(2)}$ over the master surface (Γ_m) in the current configuration as

$$g(\mathbf{X},t) = -\mathbf{n}[\mathbf{x}^{(1)}(\mathbf{X}^{(1)},t)] \cdot [\mathbf{x}^{(1)}(\mathbf{X}^{(1)},t) - \hat{\mathbf{x}}^{(2)}(\mathbf{X}^{(2)},t)]. \tag{5}$$

Together with the normal contact pressure, $\lambda_n(\mathbf{X},t)$, the gap function creates a set of conditions known as the Kuhn-Karush-Tucker (KKT) conditions, which enforce a non-penetration relation on the normal direction of Γ_c,

$$g(\mathbf{X},t) \geq 0,\ \lambda_n \leq 0,\ \lambda_n g(\mathbf{X},t) = 0. \tag{6}$$

In the tangential direction, the frictional conditions are given by the Coulomb's law:

$$\psi := |t_\tau| - \mu|\lambda_n| \leq 0. \tag{7}$$

Having stated these definitions, let $\mathbf{v}$ be virtual displacement vector and $\mathbf{V}$ the space of test functions fulfilling the condition $\mathbf{v} = 0$ on the Dirichlet boundary Γ_D. Then, applying the principle of virtual work to the boundary value problem and using the KKT conditions (6), the energy problem is reduced to finding $\mathbf{u} \subset \{\mathbf{u}_s, \mathbf{u}_m\} \in V$ such that,

$$\partial\Pi(\mathbf{u},\delta\mathbf{u}) = \partial\Pi_{int,ext}(\mathbf{u},\delta\mathbf{u}) + \partial\Pi_c(\mathbf{u},\delta\mathbf{u}) = 0, \tag{8}$$

where $\partial\Pi_{int,ext}(\mathbf{u},\delta\mathbf{u})$ represents the virtual work from the internal and external forces. The contact virtual work, $\partial\Pi_c(\mathbf{u},\delta\mathbf{u})$, is obtained by the integration – over the *slave side* – of the work done by the contact traction $\mathbf{t}_c^{(1)}$,

$$\partial\Pi_c(\mathbf{u},\delta\mathbf{u}) = -\int_{\Gamma_s} \mathbf{t}_c^{(1)} \cdot \left(\delta\mathbf{u}^{(1)} - \delta\mathbf{u}^{(2)}\right) d\Gamma_s. \tag{9}$$

The next section presents the discretization procedures adopted for solving the contact virtual work equation (9).

3 DISCRETIZATION

Since the lagrangian method has been extensively treated in the literature, the discretization procedure adopted for this method may be found in references such as Laursen [9] and Wriggers [10]. The discretization using a dual basis for the lagrangian multipliers adopted in this work is strongly based in the works of Hüeber et al. [5], Popp et al. [7] and Gitterle et al. [8], however a remark – concerning the final equation system used – must be made. Introducing the Lagrange multiplier, on the slave side, as the negative of the contact traction $\boldsymbol{\lambda} = -\mathbf{t}_c^{(1)}$ it is possible to rewrite equation (9) as,

$$\delta\Pi_c(\mathbf{u},\delta\mathbf{u},\boldsymbol{\lambda}) = \int_{\gamma_c^{(1)}} \boldsymbol{\lambda} \cdot \left(\delta\mathbf{u}^{(1)} - \delta\mathbf{u}^{(2)}\right) d\gamma \tag{10}$$

which represents a weak integral replacement of the strong pointwise non-penetration condition. The matrix form of equation (8) was reduced to the following pure displacement problem,

$$\begin{bmatrix} \mathbf{K}_{\mathcal{N}\mathcal{N}} & \mathbf{K}_{\mathcal{N}\mathcal{M}} & \mathbf{K}_{\mathcal{N}\mathcal{I}} & \mathbf{K}_{\mathcal{N}\mathcal{I}} \\ \mathbf{K}_{\mathcal{M}\mathcal{N}} + \hat{\mathbf{M}}_{\mathcal{A}}^{T}\tilde{\mathbf{K}}_{\mathcal{A}\mathcal{N}} & \tilde{\mathbf{K}}_{\mathcal{M}\mathcal{M}} + \hat{\mathbf{M}}_{\mathcal{A}}^{T}\tilde{\mathbf{K}}_{\mathcal{A}\mathcal{M}} & \tilde{\mathbf{K}}_{\mathcal{M}\mathcal{I}} + \hat{\mathbf{M}}_{\mathcal{A}}^{T}\tilde{\mathbf{K}}_{\mathcal{A}\mathcal{I}} & \tilde{\mathbf{K}}_{\mathcal{M}\mathcal{A}} + \hat{\mathbf{M}}_{\mathcal{A}}^{T}\tilde{\mathbf{K}}_{\mathcal{A}\mathcal{A}} \\ \mathbf{K}_{\mathcal{M}\mathcal{A}} & \tilde{\mathbf{K}}_{\mathcal{I}\mathcal{M}} & \tilde{\mathbf{K}}_{\mathcal{I}\mathcal{I}} & \tilde{\mathbf{K}}_{\mathcal{I}\mathcal{A}} \\ \mathbf{0} & \hat{\mathbf{M}}_{\mathcal{A}} & \tilde{\mathbf{S}}_{\mathcal{A}\mathcal{I}} & \tilde{\mathbf{S}}_{\mathcal{A}\mathcal{A}} \\ \hat{\mathbf{T}}_{\mathcal{A}}\mathbf{K}_{\mathcal{A}\mathcal{N}} & \hat{\mathbf{T}}_{\mathcal{A}}\tilde{\mathbf{K}}_{\mathcal{A}\mathcal{N}} & \hat{\mathbf{T}}_{\mathcal{A}}\tilde{\mathbf{K}}_{\mathcal{A}\mathcal{N}} - \tilde{\mathbf{F}}_{\mathcal{A}\mathcal{I}} & \hat{\mathbf{T}}_{\mathcal{A}}\tilde{\mathbf{K}}_{\mathcal{A}\mathcal{N}} - \tilde{\mathbf{F}}_{\mathcal{A}\mathcal{I}} \end{bmatrix} \begin{bmatrix} \Delta\mathbf{d}_{\mathcal{N}} \\ \Delta\mathbf{d}_{\mathcal{M}} \\ \Delta\mathbf{d}_{\mathcal{I}} \\ \Delta\mathbf{d}_{\mathcal{A}} \end{bmatrix} = \begin{bmatrix} \mathbf{r}_{\mathcal{N}} \\ \mathbf{r}_{\mathcal{M}} + \hat{\mathbf{M}}_{\mathcal{A}}^{T}\mathbf{r}_{\mathcal{A}} \\ \mathbf{r}_{\mathcal{I}} \\ \hat{\mathbf{T}}_{\mathcal{A}}\mathbf{r}_{\mathcal{A}} \end{bmatrix} \quad (11)$$

here, indexes $\mathcal{N}$, $\mathcal{M}$, $\mathcal{I}$, $\mathcal{A}$ stands for the set of internal nodes, nodes on the mortar side, inactive non-mortar nodes and active non-mortar nodes, respectively. The matrix $\tilde{\mathbf{K}}$ corresponds to the summation of the standard tangent stiffness matrix $\mathbf{K}$ and the matrix $\tilde{\mathbf{C}}$, which contains the directional derivatives of both mortar matrices $\mathbf{D}$ and $\mathbf{M}$. Matrix $\tilde{\mathbf{S}}$ contains the directional derivatives of the gap functions vector $\tilde{\mathbf{g}}$, while the matrix $\tilde{\mathbf{F}}$ is obtained by assembling the tangent vector linearizations together with the current values of the Lagrange multipliers. The matrices $\hat{\mathbf{T}}$ and $\hat{\mathbf{M}}$ are defined as, $\hat{\mathbf{T}} = \mathbf{D}^{-1}\mathbf{T}$ and $\hat{\mathbf{M}} = \mathbf{D}^{-1}\mathbf{M}$, respectively. Since friction is taken into account, the terms related to stick and slip must be considered in the tangent matrix $\mathbf{T}$. Finally, the residual force vector is computed in terms of the vector of internal forces, $\mathbf{f}_{int}$, the vector of external forces, $\mathbf{f}_{ext}$, and the contact forces, $\mathbf{f}_c$, as follows,

$$\mathbf{r} = \mathbf{f}_{int}(\mathbf{d}) + \mathbf{f}_c(\mathbf{d}, \mathbf{z}) - \mathbf{f}_{ext} = \mathbf{0}, \quad (12)$$

where $\mathbf{d}$ represents the nodal displacements and the nodal values of the lagrangian multipliers, $\mathbf{z}$, are recovered using the following relation,

$$\mathbf{z} = \mathbf{D}^{-1}\left(-\mathbf{r}_{\mathcal{I}} - \mathbf{K}_{\mathcal{I}\mathcal{N}}\Delta\mathbf{d}_N - \tilde{\mathbf{K}}_{\mathcal{I}\mathcal{M}}\Delta\mathbf{d}_M - \tilde{\mathbf{K}}_{\mathcal{I}\mathcal{I}}\Delta\mathbf{d}_I\right). \quad (13)$$

The solution is undertaken using a sparse equation solver with the Newton-Raphson method, were the residual forces are indirectly used as a control parameter. The outcome is a fast and memory-optimized solver.

4 NUMERICAL EXAMPLES

In this section a set of three numerical problems is presented. The objective of those analyzes is to compare the standard Lagrange method and the Dual Mortar method, when plastic strain comes to play. Two normal contact problems are considered first to evaluate which formulation provides better load transfer. The second example is a classical Hertzian contact problem. Lastly, a conical extrusion problem is considered. Three materials were employed in the simulations and their properties are detailed in Table 1. All the examples employ the four node quadrilateral F-BAR finite element [11] and two node linear mortar elements.

Table 1: Material properties.

Material	E	G	ν	σ_y	Hardening law
Steel ANSI 9000	210 GPa	76 GPa	0.33	830 MPa	$\sigma = \sigma_y + 600\,(\epsilon)^{0.21}$
Al ANSI 201.0(†)	71.15 GPa	26 GPa	0.30	370 MPa	$\sigma = \sigma_y + 550\,(\epsilon)^{0.223}$
Al ANSI 771.0(‡)	69.8 GPa	26.12 GPa	0.32	31 MPa	$\sigma = \sigma_y + (\epsilon)\,(G/100)$

4.1 Normal contact problems

This first case study is mainly concerned with the correct prediction of strains/stresses in the normal direction, and therefore no friction is considered. Two contact problems are chosen: the classical contact patch test (Fig. 1) and the block pile problem (Fig. 2). The contact patch test [12] is the most commonly used benchmark to evaluate the load transfer from the contacting surface (master surface) to the target surface (slave surface). Here, a point load $F = 7.2kN$ is applied on each node at the top of the structure. The objective is to generate a constant uniaxial stress field in both contact bodies. By doing this, the Ladyzhenskaya-Babuska-Brezzi (LBB) criteria (discrete version of the inf-sub condition) should be satisfied.

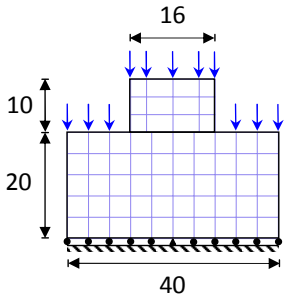

Figure 1: Contact patch test.

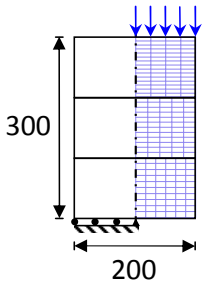

Figure 2: Block pile problem.

Another example typically employed to verify if the normal contact forces are correctly computed, is solving the block pile problem [13]. It consists of an arrangement of several blocks – with the same geometry – where a prescribed displacement (or distributed load) over the top surface of the last block on the pile is applied. The structure is meant to behave as an axisymmetric bar. Here, a prescribed displacement of $\delta_y = -15mm$ is applied to the top surface of the upper block. Since no friction is considered, the contacting surfaces should slide over each other, making the blocks deform alike. The ANSI 9000 Steel (Table 1) was employed for both problems. Applying the Lagrange Method to enforce the contact constraints in the first problem and using a single pass NTS detection to create the contact pairs will produce the results shown in Fig. 3. The displacement field, despite the excessive penetration of the contacting nodes at the corner of the slave body, have a quite smooth pattern. However, the effective stresses are not equally distributed over the structure and the formulation fails the test. The use of a double pass NTS detection approach to reduce penetration leads to the locking of the contacting surfaces. On the other hand, solving the contact constraints using the Dual Mortar Method provides an exact displacement pattern and the stress field is constant, see Fig. 4. The use of a non-linear material did not affect the quadratic convergence rate of the relative residual force.

The solution of the block pile problem also emphasized the limitations of the NTS approach, see Fig. 5. The pointwise nature of the contact enforcement, especially at the block's corner, made it very difficult to maintain the correct contact pairs. Eventually,

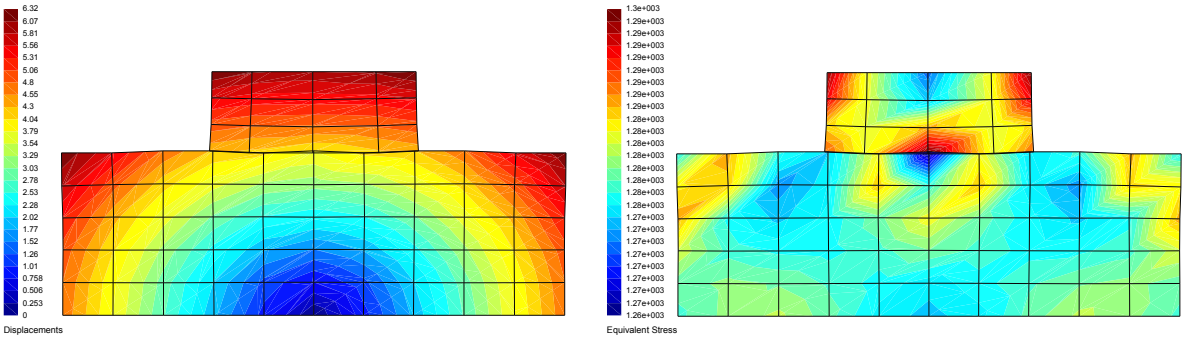

Figure 3: Contact patch test - Lagrange.

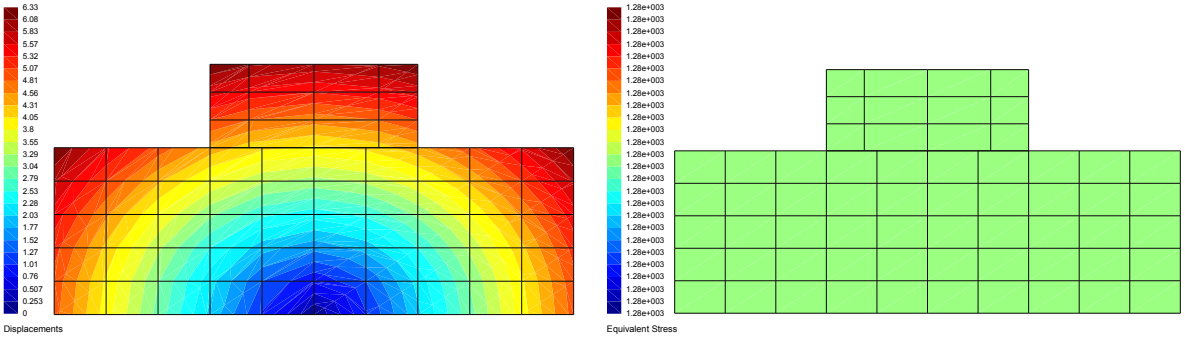

Figure 4: Contact patch test - Dual Mortar.

the corner nodes on the slave side went outside the limits of the master side domain. When this happens, the slave node is no longer enforced. High levels of penetration are reached, which also compromises the enforcement of the neighborings nodes. The results obtained by the Dual Mortar method are shown in Fig. 6. The segment-to-segment pairing, provided by the dual functions, compel the corner nodes to remain in contact. The outcome is a smooth deformation of the entire structure and a uniform uniaxial stress field.

4.2 Hertizian problem

The classical problem of Hertz is the second case of study. In this problem, a steel cylinder is pressed into an aluminium[†] block. The initial contact area is very small (non-conforming point contact) and a curved contact surface is present. The simulation is conducted as a two-dimensional plane-strain analysis. Geometry of the problem and finite element mesh are depicted in Fig. 7. Due to the symmetry, only half mesh is analyzed. The block's bottom surface is fixed. A friction coefficient of 0.1 was adopted in this analysis. The great asset of this case study relies on the existence of an analytical solution in the elastic domain. It is obtained from the Hertizian contact formulae for two

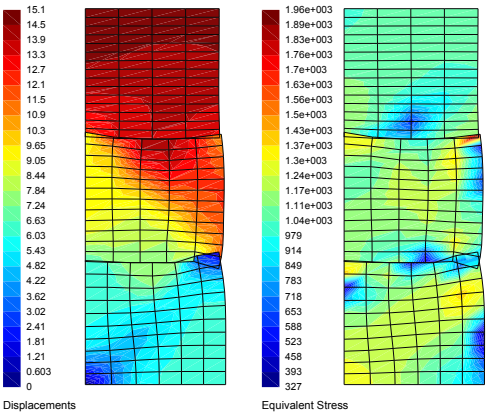

Figure 5: Block pile problem - Lagrange.

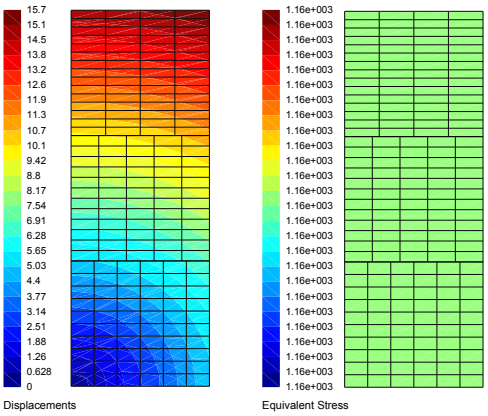

Figure 6: Block pile problem - Dual Mortar.

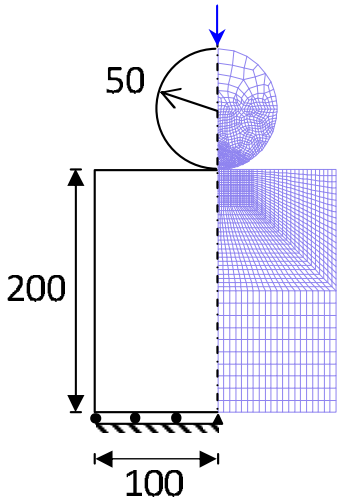

Figure 7: Hertizian problem.

cylinders, which defines the maximum contact pressure, P_{max}, the contact width, a, and the contact pressure along x-coordinate P as:

$$P_{max} = \sqrt{\frac{FE^*}{2\pi R^*}} \ , \ a = \sqrt{\frac{8FR^*}{\pi E^*}} \ , \ P = P_{max}\sqrt{1 - \left(\frac{x}{a}\right)} \tag{14}$$

where the combined elasticity modulus, E^*, is obtained from the material parameters of the punch (E_p) and the block (E_b) as follows:

$$E^* = \frac{2E_pE_b}{E_p\left(1-\nu_b^2\right) + E_b\left(1-\nu_p^2\right)} . \tag{15}$$

and the combined radius, R^*, is evaluated from the radius of the cylinder, R_1, and block, R_2, in a similar way, but since $\Rightarrow R_2 \rightarrow \infty$, the combined radius is reduced to the cylinder's radius,

$$R^* = \lim_{R_2 \to \infty} \frac{R_1 R_2}{R_1 + R_2} = \lim_{R_2 \to \infty} \frac{R_1}{R_1/R_2 + 1} = R_1. \tag{16}$$

In order to compare the numerical results and analytical solution, the analysis was divided in two phases. In a first moment, a compressive point load $F = 5kN$ is applied to the top of the cylinder. Under this load, only elastic strains will manifest, which allows a direct comparison with the analytical solution. For the given numerical parameters, the expected results are: $P_{max} = 1577.32N/mm^2$; $a = 2.018mm$; and $P = 1577.32\sqrt{1 - \left(\frac{x}{a}\right)^2}$.

In the second phase of the analysis, the point load is raised to $F = 12.5kN$, which leads to the appearance of plastic strains on both sides of the contact surface. The frictional forces becomes more significant, making the limitations of the NTS discretization more evident.

4.2.1 Elastic strains

In the first phase of the case study, the applied load yields a maximal Equivalent Stress at $x = 0$ equal to $327kN/mm^2$. This pressure is below the yield stress of both material employed, which assures that no plastic strains are in place. Also at this point, frictional forces are negligible. The load is well transfered and a Relative Residual Norm of E-10 is quadratically achieved after 4 iterations for the Lagrange method and 3 iteration for the Dual Mortar method. A comparison between the analytical solution and the results provided by the numerical simulations is depicted in Fig. 8. Despite the oscillation of the normal forces both results have a reasonable agreement.

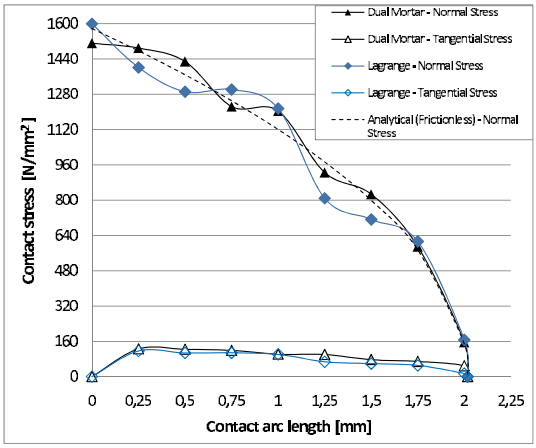

Figure 8: Contact stress - Elastic strains.

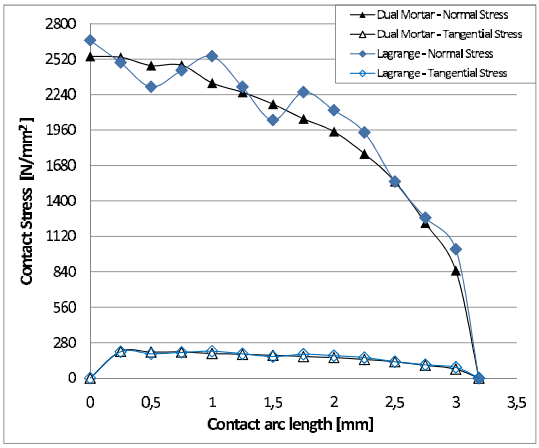

Figure 9: Contact stress - Plastic strains.

4.2.2 Plastic strains

On to the second phase, under the action of a vertical force of 12.5kN, the contact surface includes plastic deformation and the friction forces becomes considerably higher. Results are shown in Fig. 9 and Table 2. The stress distribution predicted by the NTS-

Table 2: Results of Hertizian problem - Plastic strains.

		Lagrange	Dual Mortar
TOTAL DISPLACEMENT [mm]	Cylinder	0.433	0.431
	Block	0.432	0.431
AVERAGE DEFORMATION	Cylinder	0.184	0.182
	Block	0.416	0.431
CONTACT LENGTH [mm]		3.178	3.198
Increment	Iteration	Relative residual norm (%)	
1	1	0.575085E-01	0.836091E-02
	2	0.140132E-04	0.739726E-06
	3	0.212436E-06	0.922262E-10
	4	0.172358E-10	
100	1	0.213476E-01	0.223108E-03
	2	0.510660E-04	0.198341E-07
	3	0.399832E-09	0.135704E-11
	4	0.340939E-12	
200	1	0.354716E-01	0.754524E-04
	2	0.485938E-03	0.917062E-08
	3	0.337746E-06	0.896271E-12
	4	0.852251E-11	

Lagrange method is no longer liable. Oscillations of normal forces reduced the results accuracy. The convergence rate is also decreased. On the other hand, since the number of contacting nodes increased, the results obtained using the Dual Mortar method have a better distribution of loads over the contact surface. Normal and tangential forces follow a relatively smoother pattern and convergence rate remained faster.

4.3 Conical extrusion

The problem undertaken in this example is an elasto-plastic stress analysis of an aluminium[‡] cylindrical billet. The billet is pushed a total distance of 177.8mm through a rigid conical die which has a wall angle of 5 degrees, see Fig. 10. The objectives are to predict the displacement of the billet material, the forces generated during the extrusion process and also the effective plastic strain distribution of the deformed billet. By analyzing the evolution of these variables it is also possible to assess the performance of

the Lagrangian Method and the Dual Mortar method when the contacting body is in the presence of frictional forces and plastic strains.

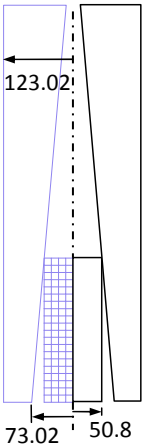

Figure 10: Conical extrusion - Geometry.

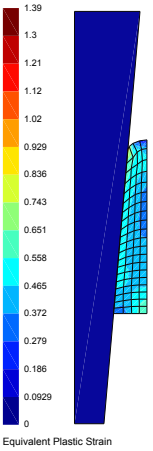

Figure 11: Conical extrusion - Plastic Strain.

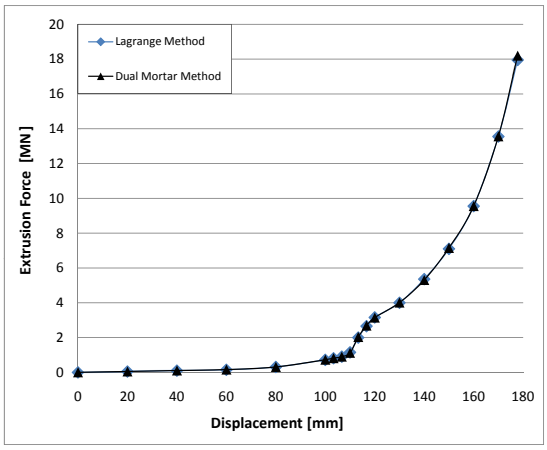

Figure 12: Extrusion forces.

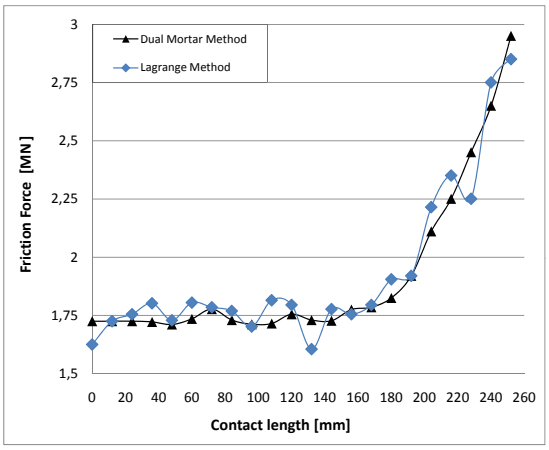

Figure 13: Frictional forces.

The Equivalent Plastic Strain obtained by the Dual Mortar method is shown in Fig. 11. The higher plastic deformation is found at the upper left side of the billet with a maximal value of 1.39. The final contact surface length is 257.33mm. A graphical representation of the extrusion force (measured from the reaction at the billet bottom) is shown in Fig. 12, the deviation between the two methods is very small. The convergence rate achieved was similar to the one obtained in section 4.2.2. Nevertheless, the evolution of the friction forces obtained by the Lagrangian method, see Fig. 13, shows the typical oscilation, which is due to the finite element discontinuities along the contact surface. This

drawback is mitigated by the segment-to-segment approach of the Dual Mortar method, which performs better.

5 CONCLUDING REMARKS

The results presented emphasize the benefits of using a dual basis for the lagrangian multipliers. The evaluation of the gap function as a semi-continuous weak integral yields a much better enforcement of constraints in the normal direction. This advantage leads to a more accurate evaluation of the contact forces, not only in the normal direction but also the reactions in the tangential direction as well. Additionally, it contributes to the correct fulfillment of the additional nonlinearity sources, i.e. sharp contact, friction plastic strain and friction forces. Furthermore, the superior correlation between the contacting bodies will promote a smaller initial value for the residual forces which will lead to a faster solution. The results suggest that the use of a higher order finite element/mortar element would also improve the effectiveness of the method, especially when dealing with sharp contact surfaces and curved surfaces. Such an improvement is necessary for solving contact problems between solids with irregular surfaces and with a higher friction coefficient, which may be a topic for future work.

REFERENCES

[1] C. Bernardi, Y. Maday, A. Patera, "*A new nonconforming approach to domain decomposition: the mortar element method*", in: H. Brezia, J. Lions (Eds.), Nonlinear Partial Differential Equations and their Applications, Pitman and Wiley, 1992, pp. 13-51.

[2] M.A. Puso, T.A. Laursen and J. Solberg, "*A segment-to-segment mortar contact method for quadratic elements and large deformations*", Comput. Methods. Appl. Mech. Engrg. (2008); 197: 555-566.

[3] M. Tur, F.J. Fuenmayor and P. Wriggers, "*A mortar-based frictional contact formulation for large deformations using Lagrange multipliers*". Comput. Methods Appl. Mech. Engrg, (2009); 198: 2860-2873.

[4] B. Wohlmuth. "*A mortar finite element method using dual spaces for the Lagrange multiplier*". SIAM Journal on Numerical Analysis (2000); 38: 989-1012.

[5] S. Hüeber and B.I. Wohlmuth. "*A primal-dual active set strategy for non-linear multibody contact problems*". Comput. Methods Appl. Mech. Engrg(2005); 194: 3147-3166

[6] S. Hartmann, S. Brunssen, E. Ramm and B. Wohlmuth. "*Unilateral non-linear dynamic contact of thin-walled structures using a primal-dual active set strategy*". Int. J. Numer. Meth. Engng. (2007); 70: 883-912.

[7] A. Popp, M.W. Gee and W.A. Wall. "*A finite deformation mortar contact formulation using a primal-dual active set strategy*". Int. J. Numer. Meth. Engng. (2009); 79: 1354-1391.

[8] M. Gitterle, A. Popp, M.W. Gee and W.A. Wall. "*Finite deformation frictional mortar contact using a semi-smooth Newton method with consistent linearization*". Int. J. Numer. Meth. Engng (2010); 84: 543-571.

[9] T.A. Laursen, "*Computational Contact and Impact Mechanics: Fundamentals of Modeling Interfacial Phenomena in Nonlinear Finite Element Analysis*", Springer-Verlag, Heidelberg (2002).

[10] P. Wriggers, "*Computational Contact Mechanics*", John Wiley & Sons, 2002.

[11] E.A. de Souza Neto, D. Perić, M. Dutko, and D.R.J. Owen, "*Design of Simple Low Order Finite Elements for Large Strain Analysis of Nearly Incompressible Solids*". Int. J. Solids Structs (1996); 33, 3277-3296.

[12] R.L. Taylor and P. Papadopoulos. "*On a patch test for contact problems in two dimensions. Computational Methods in Nonlinear Mechanics*", Wriggers, P. and Wagner, W., Springer-Verlag, pages 670-702, 1991.

[13] T.A. Laursen et al., "*Mortar contact formulations for deformable-deformable contact: Past contributions and new extensions for enriched and embedded interface formulations*", Comput. Methods Appl. Mech. Engrg. (2010), doi:10.1016/j.cma.2010.09.006